UNIVERSITY *of York*

This is a repository copy of *A Highly Stable and Sensitive MEMS-based Gravimeter for Long-term Earth Tides Observations*.

White Rose Research Online URL for this paper:
https://eprints.whiterose.ac.uk/id/eprint/191621/

Version: Accepted Version

Article:

White Rose
university consortium
Universities of Leeds, Sheffield & York

eprints@whiterose.ac.uk
https://eprints.whiterose.ac.uk/

A Highly Stable and Sensitive MEMS-based Gravimeter for Long-term Earth Tides Observations

Lujia Yang, Xiaochao Xu, Qian Wang, Ji'ao Tian, Yanyan Fang, Chun Zhao, *Senior Member, IEEE*, Fangjing Hu and Liangcheng Tu

Abstract—**Precision measurements of local gravitational acceleration variations are of great importance in geophysical surveys. With advantages such as cost-effectiveness and portability, Micro-Electro-Mechanical system (MEMS)-based gravimeters have shown the potential for long-term gravity measurements. In this paper, aiming to further improve the stability of the instrument, the design considerations and system evaluations of a MEMS gravimeter are presented. With a linear spring design for the silicon proof-mass, a low natural frequency of ~14 Hz and a large linear range of ~10300 mGal are achieved with an ultra-low self-noise floor of 1.2 µGal/√Hz@1 Hz. By implementing a vacuum chamber system, the pressure variation is reduced from hundreds of Pa/day in atmosphere to a linear variation of ~6 Pa/day. In addition, an active temperature control system can suppress temperature fluctuations by 2 to 3 orders of magnitude within the band from 1×10^{-4} Hz to 1×10^{-2} Hz. The stability of the proposed MEMS gravimeter is demonstrated via long-term Earth tides observations within a 30-day time span, giving a correlation coefficient of 0.957 with the reference. An excellent bias instability of ≤4 µGal is demonstrated within the 8-3000 s averaging time range, representing one of the best performances to date in terms of stability for MEMS gravimeters. This shows the potential of high-performance MEMS gravimeters for petroleum and mineral prospecting, seismology and other geophysical applications.**

Index Terms— **Micro-Electro-Mechanical system (MEMS), gravity sensor, gravimeter, Earth tides.**

I. INTRODUCTION

High precision gravimeters have found important applications in carbon sequestration [1], [2], mineral exploration [3], geology [4], volcanology [5], and groundwater storage monitoring [6] based on the sub-surface density anomalies derived from the gravity data. In general, gravimeters can be divided into absolute and relative types, depending on the principle used to measure gravitational accelerations. Absolute gravimeters determine the absolute values of gravitational accelerations by measuring the trajectory of the test mass in a free-fall experiment. Typical commercial absolute gravimeters (e.g., Micro-g Lacoste FG5-X) show a

resolution of ~0.1 µGal and excellent long-term stabilities, and, therefore, have been used to establish long-term stable references and calibration lines for relative gravimeters [7]. However, absolute gravimeters are not suitable for field-portable gravity surveys due to the bulky size and high cost. On the other hand, relative gravimeters obtain the relative variations of gravitational accelerations by measuring the displacement of a spring-mass structure. State-of-the-art relative gravimeters such as Scintrex CG-6 can achieve a reading resolution of ~0.1 µGal and a good stability, providing sufficient performances for both static and transportable gravity measurements. In addition, by employing superconducting technologies, GWR superconducting gravimeters demonstrate an ultra-low noise floor of 0.3 µGal/√Hz and a precise of 0.05 µGal in the time domain with 1 minute averaging [8].

Over the past decades, with the development of micro-fabrication technologies, a large variety of Micro-Electro-Mechanical system (MEMS)-based inertial sensors have been developed, showing advantages such as portability, mass production, low power consumption and cost effectiveness [9]-[13]. Among which, MEMS accelerometers with micro-structured silicon spring-mass systems have found applications in inertial navigation [14], [15], consumer electronics [16], and seismic monitoring [17], [18]. The resolutions of MEMS accelerometers have been greatly improved from mg/√Hz regime for consumer electronics applications to sub-ng/√Hz, enabling the measurements of micro-seismic signals in the InSight mission [19]. Although the ever-improving performances of MEMS inertial sensors make it possible to be used for high-precision gravity measurements in terms of the sensitivity, it is not readily available to perform long-term Earth tides observations using such devices unless the stability can be increased.

Extensive efforts have been made to improve the sensitivity and stability of MEMS sensors, as well as to establish temperature and pressure stable environments, for long-term gravity measurements. In 2016, Middlemiss *et al.* reported a MEMS gravity sensor composed of an anti-spring suspension

with an ultra-low natural frequency f_0 = 2.3 Hz and an optical shadow transducer. The MEMS sensor was assembled into a temperature-controlled vacuum system, and successfully measured the Earth tides, making the transition from the accelerometer to the gravimeter [20]. To facilitate the device miniaturization, an updated MEMS gravimeter by employing a capacitive displacement transducer was demonstrated with an improved stability [21]. By combining the folded beams with curved beams, as well as to construct a vacuum chamber shielded by thermal insulation materials, Tang *et al*. reported a MEMS gravimeter with a larger dynamic range of 8000 mGal [22]. However, the structures in [20]-[22] employ quasi-zero springs with low natural frequencies to improve the sensitivity of the MEMS gravity sensors, resulting in a high requirement for the fabrication and installation of the MEMS gravimeters in practical use. To tackle this problem, a MEMS gravity sensor with a linear spring design (f_0 = 14 Hz) and a capacitive displacement transducer was developed by Xu *et al*., and successfully observed Earth tide signals in an atmosphere environment by removing the effect of the ambient pressure fluctuations within a temperature-controlled system [23]. In addition to MEMS gravity sensors that are typically based on displacement transducers, MEMS devices based on vibrating elements can also be used to gravity measurements by tracking the frequency shift of the element. A wafer-level vacuum encapsulation of a vibrating beam MEMS accelerometer with a three-stage temperature control was proposed by Mustafazade *et al*., and recorded the Earth tides and teleseismic events, validating its capability for gravity measurements [24]. More recently, by optimizing the resonator, micro-level and suspension beam structures, a resonant MEMS accelerometer

sealed in a hermetic ceramic case within a temperature control chamber was demonstrated by Zheng *et al*. with a bias stability of 0.197 µg/day [25].

Unfortunately, most of the previous studies emphasize on the improvements of the MEMS gravity sensors. Since the MEMS sensors are sensitive to the temperature and pressure variations, the effects of the environmental change are dominating factors to the stability of the MEMS gravity sensor. Therefore, it is also essential to perform systematical investigations on the temperature and pressure effects to improve the stability of MEMS gravity sensors, and to serve as a guide for further developments of MEMS gravimeters. In this paper, the design considerations and evaluations of a MEMS gravimeter system is presented. A vacuum chamber and a temperature control system are designed to suppress the pressure and temperature fluctuations, respectively, providing a stable environment for the MEMS gravity sensor. The long-term Earth tides measurement within a time-span of 30 days exhibits a correlation coefficient of 0.957 with the reference data, and an excellent stability with a bias instability of ⩽4 µGal within an averaging time from 8 s to 3000 s, representing one of the best performances to date for MEMS gravimeters.

II. DESIGN AND EVALUATION OF THE MEMS GRAVIMETER

In this section, the design considerations and evaluations of a MEMS gravimeter will be demonstrated in detail. A vacuum chamber as well as a high-precision temperature control system are implemented to provide a stable test environment for the gravity sensor.
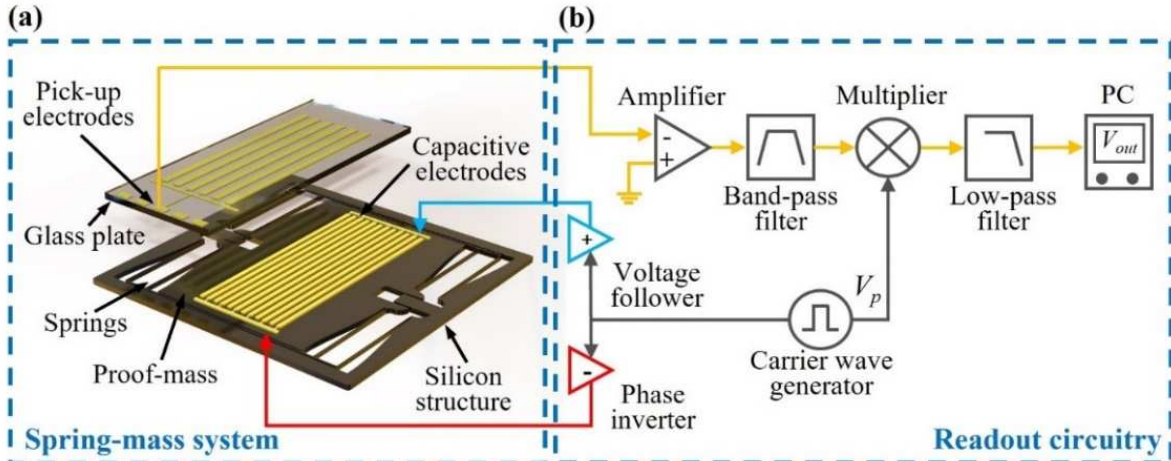
Fig. 1. Schematic diagram of the MEMS gravity sensor and the processing circuitry. (a) Schematic diagram of the spring-mass system. The silicon-based mechanical structure comprises a proof-mass suspended by folded springs. The proof-mass has capacitive electrodes electroplated on its surface, while the pick-up electrodes are electroplated on a glass plate. (b) Readout circuitry of the MEMS gravity sensor.

A. MEMS Gravity Sensor

The MEMS gravity sensor consists of a silicon-based spring-mass system and a readout circuitry, as shown in Fig. 1. Since the gravity signal of interest is ultra-low in frequency (e.g., the

Earth tides signals is ~1×10^{-5} Hz), a low natural frequency, thus a low stiffness for the silicon spring is preferred in order to improve the sensitivity of the MEMS gravity sensor. However, a trade-off has to be made between the spring stiffness and the robustness of the silicon spring, considering the fabrication and

installation requirements. In addition, since a large linear range of > 8000 mGal is desired for worldwide deployment, a folded spring design that could release axial force well to acquire linear relation between the acceleration signal and the displacement of the proof-mass was employed. A 500 μm thick silicon wafer was used to fabricate the spring-mass system to reduce the mechanical thermal noise, which is inversely proportional to the mass of the proof-mass system. The silicon spring was optimized to have a width of 17 μm and length of 7 mm, giving a natural frequency of ~14 Hz for the spring-mass system. The spring-mass structure with a final size of $20 \times 20 \times 0.5$ mm^3 was fabricated via a through-wafer deep reactive-ion etching technique [26]. Detailed fabrication process can be found in Note S1 of Supplemental Material.

The displacement of the proof-mass according to the external acceleration is detected by a capacitive transducer. To employ the area-varying capacitive sensing, 70 sets of interdigitated capacitive electrodes were electroplated on the silicon proof-mass, and 70 sets of pick-up electrodes were manufactured on the glass plate to detect the capacitance signals, as shown in Fig. 1(a). The glass plate was bonded on the silicon structure, and the pick-up electrodes are well aligned with the capacitive electrodes [27]. The capacitance signal is further processed by a readout circuitry, as shown in Fig. 1(b). Since the capacitance signal is weak, and is low in frequency, the lock-in detection scheme [28] is used here to suppress the low frequency noise. A 50 kHz square wave was produced by a carrier wave generator. Through a voltage follower and a phase inverter, two

square carrier waves with a phase difference of π were applied onto the inputs of the capacitance electrodes. The modulated capacitance signal from the pick-up electrodes was then fed to an operational amplifier (AD8610) with a sensitivity of 2.5 V/pF. The output of the amplifier passed through a band-pass filter within a band from 38 kHz to 62 kHz, and then to the multiplier to demodulate the signal. The demodulated signal was fed into a low-pass filter with a cutoff frequency of 24 Hz, and then logged onto a PC via a data acquisition system with a sampling frequency of 100 Hz.

B. Vacuum Chamber System

The change in atmospheric pressure can affect the output of the MEMS gravity sensor in the form of the buoyant force, leading to a gravity-pressure coefficient of 501.5 μGal/hPa [23]. This possesses one of the major error sources for MEMS gravity sensors operating in atmospheric environment, especially considering the inaccuracy in the measurement of atmospheric pressure to remove the buoyant force effect. Therefore, a stable vacuum environment is required to suppress the effect of atmospheric pressure variations. A vacuum chamber system with a core size of 16 cm × 16 cm × 16 cm was designed for the assembly of the MEMS gravity sensor, as shown in Fig. 2(a). Six exchangeable flanges that contain either a hermetic feedthrough for signal transmission, or a vacuum valve to connect a vacuum pump, or neither are included. Four lifting rings and four landing legs, at the top and the bottom, respectively, are employed to increase the portability of the MEMS gravimeter.
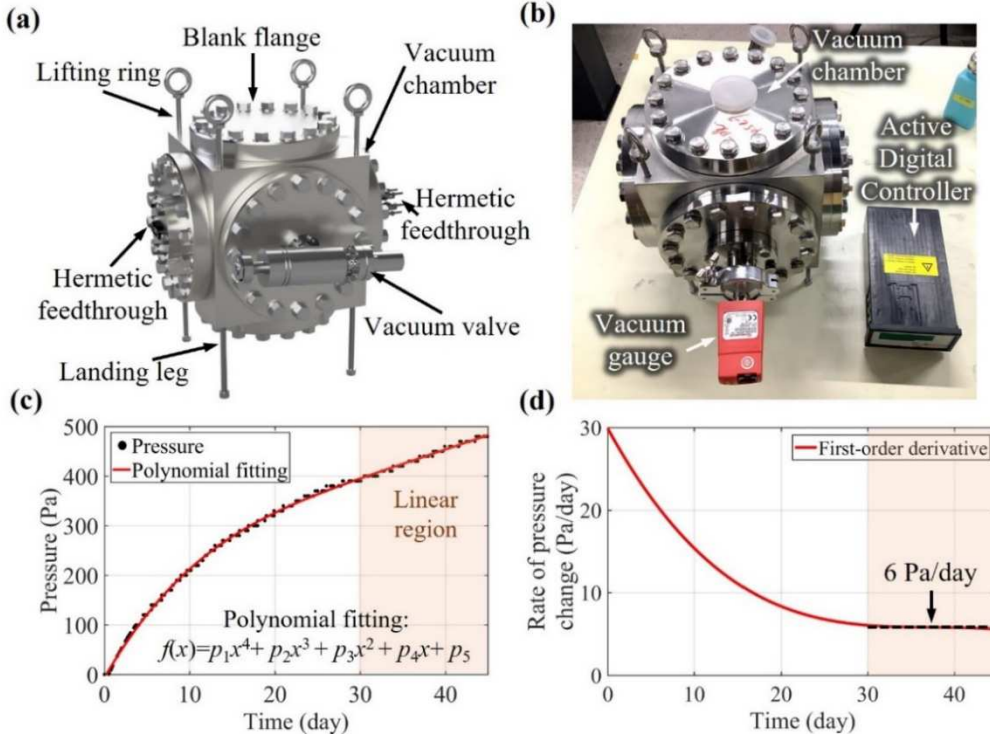
Fig. 2. Schematics and performance evaluation of the vacuum chamber system. (a) 3D model of the vacuum chamber. A steel cube is $16 \times 16 \times 16$ cm^3 in size with six exchangeable flanges. (b) Experimental setup for the monitoring of pressure variation in the vacuum chamber. (c) Measured pressure data against time for 47 days and polynomial fitting. (d) Rate of pressure change within 47 days. After 30 days, the rate of pressure change tends to be stable which is ~6 Pa/day.

The experimental setup to evaluate the performance of the vacuum chamber system by monitoring the pressure variation for 47 days is shown in Fig. 2(b). Limited by the resolution and range of the vacuum gauge (APG100-XM, EDWARDS), only pressure above 0.1 Pa can be measured with two significant digits. The vacuum chamber was first pumped down to 9.2×10^{-4} Pa using a turbo pumping system. The pressure variations in the vacuum chamber and a polynomial fitting are illustrated in Fig. 2(c). It is found that the pressure changed rapidly in first one or two weeks and tends to be linear after ~30 days. Taking the derivative of the polynomial curve fitting (Fig. 2(d)), a pressure change rate of ~6 Pa/day can be obtained in the linear region. With the vacuum chamber, the pressure variation around the MEMS gravity sensor can be reduced from hundreds of Pa/day in atmosphere to a linear variation of tens of Pa/day, giving an output of ~30 μGal/day contributed by the pressure change. The linear drift due to the pressure change then can be corrected in the data processing stage.

C. Temperature Control

The MEMS gravity sensor is temperature sensitive due to the change of the stiffness of the silicon spring, contributing to the output of the sensor. The spring stiffness k can be expressed as:

$$k = \frac{2Eb^3h}{L^3} \tag{1}$$

where E is Young's modulus of silicon (130 GPa [29], [30]), b and h are width (17 μm) and length (500 μm) of the spring section respectively, and L is the length of spring beam (7 mm). Taking the derivative of (1) with respect to temperature and dividing both sides by k, we have

$$\frac{1}{k}\frac{dk}{dT} = \frac{1}{E}\frac{dE}{dT} + \frac{3}{b}\frac{db}{dT} + \frac{1}{h}\frac{dh}{dT} - \frac{3}{L}\frac{dL}{dT} \tag{2}$$

It can be seen that the temperature coefficient of the spring stiffness comprises the contribution of the Young's modulus (-80 ppm/K [29] to -60 ppm/K [30]) and the thermal expansion coefficient of silicon (2.6 ppm/K [31]). Considering that the fixture for installation and other parts that may introduce additional temperature effects, the overall temperature coefficient of the assembled MEMS gravity sensor was measured to be 87.3±3.3 μGal/mK in our case. Temperature fluctuations within the ~mK range will result in an output of tens or hundreds of μGal, confirming that a temperature control system with ~mK precision is required for long-term gravity measurements.
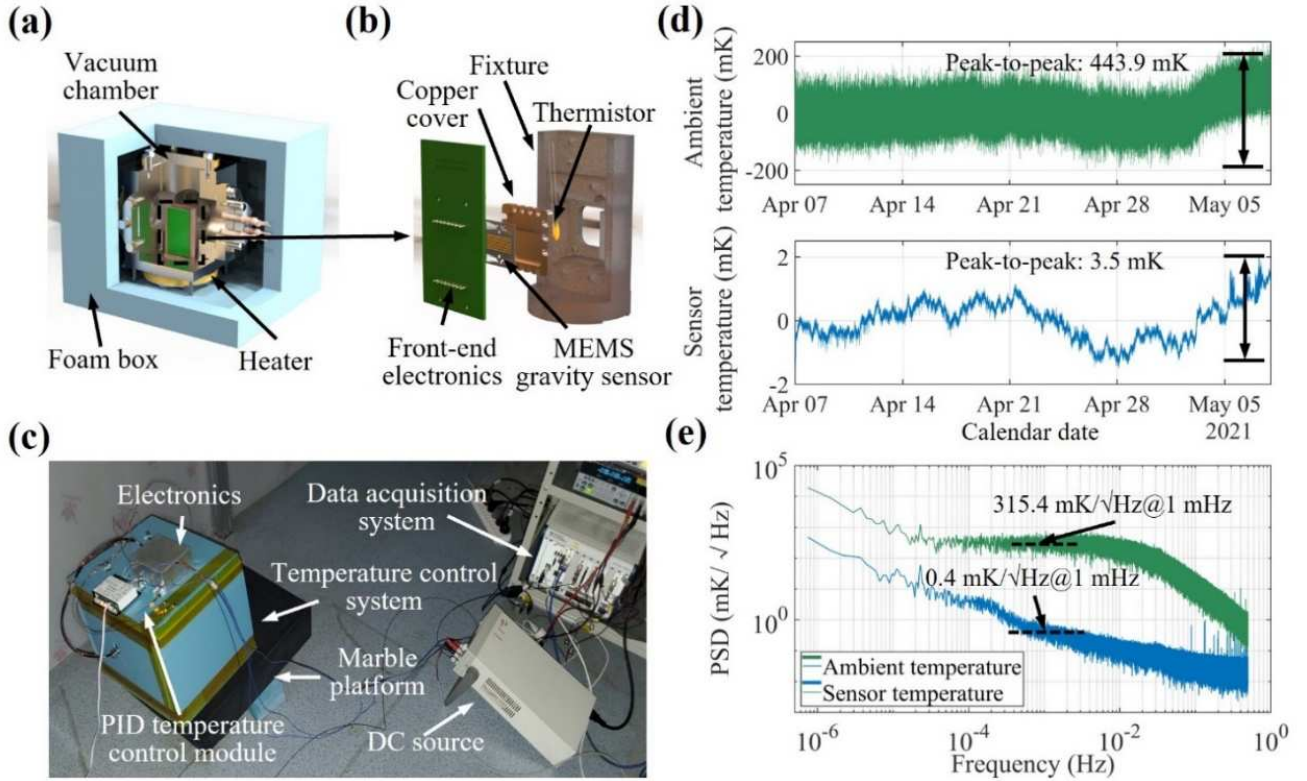
Fig. 3. Performance evaluations of the temperature control system. (a) 3D model of the temperature control system. The outer foam box with dimensions of $35 \times 30 \times 27$ cm³ serves as a passive thermal insulation layer. The assembled MEMS gravity sensor is mounted within the vacuum chamber. (b) 3D model of the MEMS gravity sensor assembly. (c) Experimental setup of the MEMS gravimeter, for which the temperature control system is placed on a marble platform. (d) Ambient and MEMS sensor temperature fluctuations for 30 days, with a peak-to-peak temperature change of 443.9 mK and 3.5 mK, respectively. (e) Power spectral densities (PSDs) of the temperature data show a suppression of 2 to 3 orders of magnitude within the band from 1×10^{-4} Hz to 1×10^{-2} Hz.

An active temperature control system and a two-stage passive thermal insulation structure were implemented to provide a temperature-stable environment, as shown in Fig. 3(a). The outermost part of the system is a rectangular box made of foam with an overall size of 35 cm × 30 cm × 27 cm for passive thermal isolation of the vacuum chamber. The active control system was implemented with a controlled temperature point of 31.4°C, for which the temperature increase is achieved by heating up the polyimide (PI) film heaters placed on the six flanges, while the temperature decrease is achieved by passive thermal dissipation when the ambient temperature is above the set value. A commercial temperature control module (TCM-M207, Oeshine) was used to control the on/off of the PI film heaters to achieve a dynamic balance with an optimum stability of ±2 mK. The assembled MEMS gravity sensor is placed inside of the vacuum chamber, as shown in Fig. 3(b). A copper cover is used to reduce the temperature gradient and to protect the MEMS gravity sensor. Due to a good thermal conductivity of the copper layer, a uniform temperature distribution can be expected within the core area around the MEMS gravity sensor. In addition, a custom fixture made from fused silica was used to further reduce the influence of non-uniform temperature distributions due to its low thermal expansion of $4.1 \times 10^{-7} K^{-1}$ [32]. Temperature fluctuations around the MEMS gravity sensor were monitored using a thermistor attached to the copper cover by thermally conductive silicone grease with a thermal conductivity of 1.93 W/(m·K).

The MEMS gravimeter for performance evaluations is shown in Fig. 3(c). The temperature control system was placed on a marble platform, accompanied with the electronics and the temperature control module TCM-M207. Temperatures were measured at a sample rate of 1 Hz. As shown in Fig. 3(d), for a peak-to-peak of ambient temperature fluctuation of 443.9 mK within 30 days, the peak-to-peak of temperature fluctuation around the MEMS gravity was about 3.5 mK. The power spectral densities (PSDs) for these two temperature data are shown in Figure 3(e), which is 0.4 mK/√Hz@1 mHz and 315.4 mK/√Hz@1 mHz for the inner temperature and the ambient temperature, respectively. The peaks at 2.3×10^{-5} Hz for both series represent the temperature change over a diurnal period. Therefore, the temperature fluctuations have been suppressed by 2 to 3 orders of magnitude within the band from 1×10^{-4} Hz to 1×10^{-2} Hz, with a PSD of less than 10 mK/√Hz for the MEMS gravity sensor.

D. Calibration and Characterization

The MEMS gravity sensor was calibrated by the tilt method [33], [34] using a biaxial dividing head with a precision of ±1 arcsecond. As shown in Fig. 4(a), the MEMS gravity sensor was fixed on the dividing head with its sensitive axis (Z axis) perpendicular to the mounting surface, and the normal direction of the proof-mass is defined as the X axis. The dividing head can provide a variable gravitational field by rotating it with an increment of 0.2 degree at each point. The relationship between the voltage output of the MEMS gravity sensor and the acceleration is shown in Fig. 4(b), and can be expressed as:

$$V = k_1 \cdot g_{acc} + k_0 \tag{3}$$

where V is the output of the MEMS gravity sensor, k_0 is the bias of sensor, g_{acc} is the gravitational acceleration provided by the dividing head. The scale factor (k_1) of the MEMS gravity sensor is determined to be 1539 V/g with the R-square of ~0.999. The linear range is estimated to be 10346 mGal.
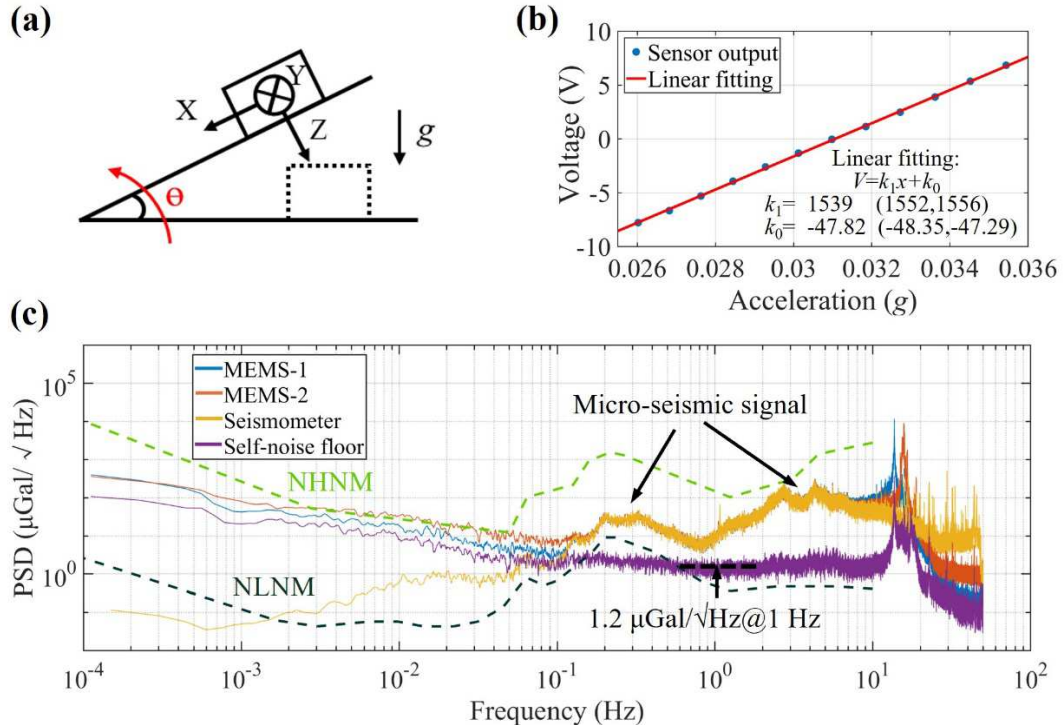

Fig. 4. Characterizations of the MEMS gravity sensor. (a) Schematic of the calibration method. (b) The scale factor and range of the MEMS gravity sensor. (c) Self-noise floor of the MEMS gravity sensor obtained by the coherence analysis method.

Since the self-noise of the MEMS gravity sensor is lower than the ambient vibration noise due to earth tremors according to the Earth's new high noise model [35], the coherence analysis method [36] was employed to obtain the self-noise floor of the MEMS gravity sensor by removing the common-mode signal of two identical MEMS gravity sensors, which are denoted as MEMS-1 and MEMS-2 in Fig. 4(c). A commercial seismometer (CMG-3ESPC, Güralp) was used to identify the angular misalignment of the sensitive axis between the two MEMS gravity sensors [37]. Fig. 4(c) shows the PSDs of the MEMS gravity sensors represented by the blue and orange solid lines, the yellow solid line denotes the PSD of CMG-3ESPC, while the dotted lines are corresponding to the Earth's new high noise model (NHNM) and the new low noise model (NLNM) respectively. The micro-seismic peaks due to earth tremors between 0.1-0.4 Hz and 2-5 Hz are clearly identified by the two MEMS gravity sensors, showing excellent agreements with the seismometer. The self-noise floor of the MEMS gravity sensor is about 1.2 µGal/√Hz@1 Hz, and is <4 µGal/√Hz within the 0.1-10 Hz band, which further confirms a high sensitivity for the MEMS gravity sensor.
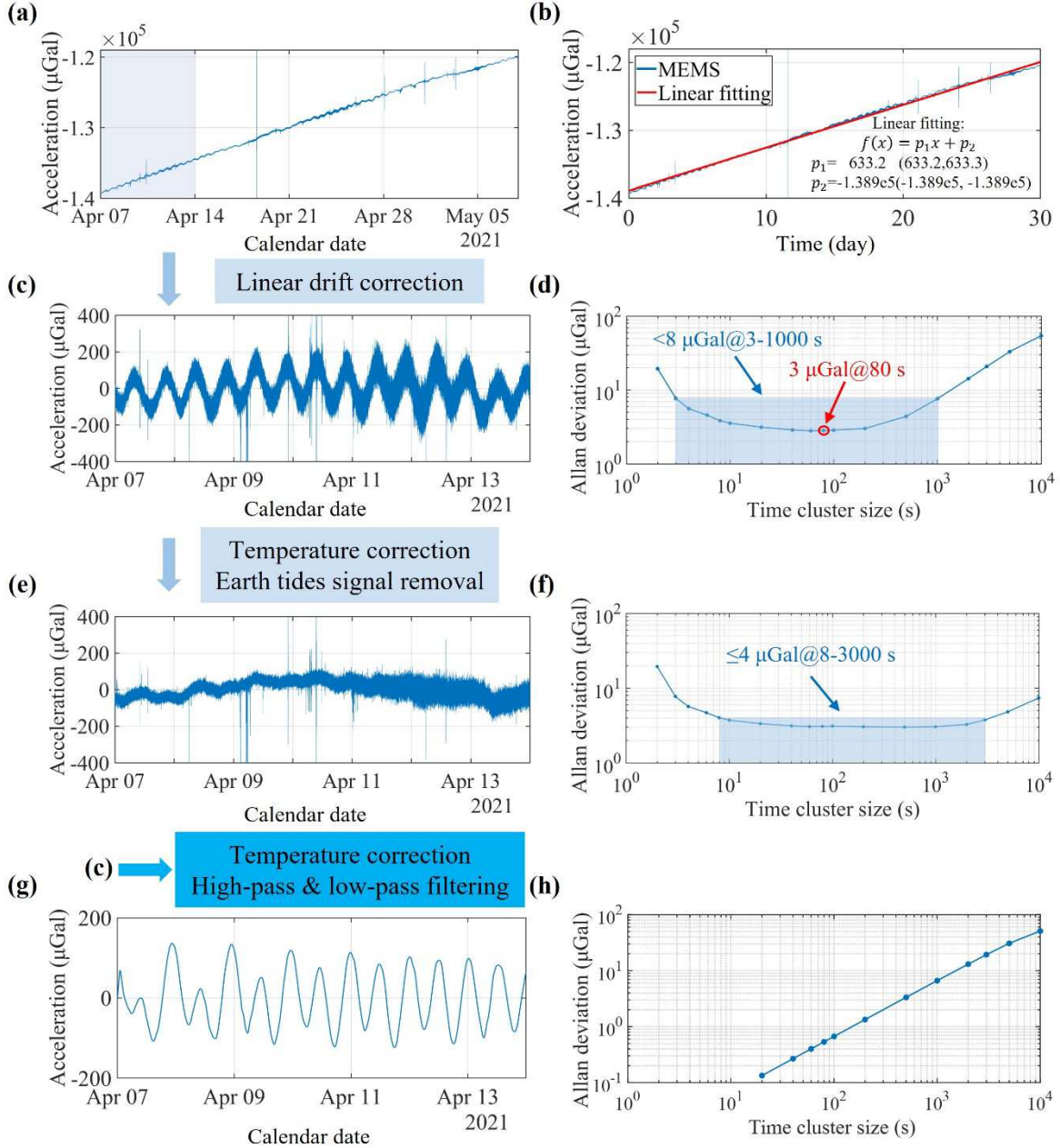

Fig. 5. Analysis procedures and corresponding results using raw data within a time-span of 30 days. (a) Raw data from April 07 to May 07, 2021, recorded at a sampling frequency of 1 Hz. (b) Linear fitting of raw data obtaining a drift rate of 633.2 µGal/day for the MEMS gravimeter. (c) Data from April 07 to 14 with a time span of 7 days after linear drift correction. (d) Allan deviation of data in (c). (e) Data in (c) after temperature correction and the Earth tides signal (recorded by a gPhoneX commerical gravimeter) removal. (f) Allan deviation of data in (e) providing a bias instability of ≤4 µGal@8-3000 s for the MEMS gravimeter. (g) Data in (c) after temperature correction, high-pass and low-pass filtering. (h) Allan deviation of data in (g).

III. Lone-term Performance Evaluation of the MEMS Gravimeter

A. Stability Evaluation

Earth tide, which is a tiny and periodic signal with an amplitude of ~300 µGal, can be used to assess the sensitivity and stability of a gravimeter. Our MEMS gravimeter has been working continuously from October 10, 2020. Experiments were conducted in a cave laboratory with a low background noise to evaluate the drift characteristics and stability of the MEMS gravimeter. A commercial gravimeter (gPhoneX) was placed co-site as a reference. Raw data, from April 07, 2021 to May 07, 2021, were selected for further analysis. As the frequency below 1×10^{-4} Hz is the frequency band of interest for a gravimeter [38], the original data with a sampling frequency of 100 Hz was decimated to 1 Hz in order to remove the high-frequency noise, as shown in Fig. 5(a). A linear drift of 633.2 µGal/day with an R-square coefficient of 0.998 was obtained, as seen in Fig. 5(b).

The sensitivity and stability of the MEMS gravimeter in the time domain can be evaluated by the Allan deviation [39]. Here, we use the one-week data from April 07 to 14 as an example to demonstrate the process for evaluating the performances of the MEMS gravimeter. Fig. 5(c) shows the raw data after the removal of the linear drift, clearly showing a semi-diurnal period signal, indicating the successful measurement of the Earth tides. The Allan deviation of the data set is shown in Fig. 5(d), showing a bias instability of <8 µGal for an integration time from 3 s to 1000 s. The residual after the removal of temperature fluctuations and the Earth tides signal is shown in Fig. 5(e), giving a bias instability of ≤4 µGal for an integration time from 8 s to 3000 s, as shown in Fig. 5(f). This demonstrates an extremely high stability of the MEMS gravimeter. However, it can be seen that the data in Fig. 5(e) still shows non-linear properties. In order to extract the Earth tides signal measured by the MEMS gravimeter, the data in Fig. 5(c) is further corrected by temperature correction, and filtered by a high-pass filter and then a low-pass filter with a cut-off frequency of 1×10^{-5} Hz and 0.1 mHz, respectively, which is as shown Fig. 5(g).

B. Earth Tides Measurements

Following the same data process, the results within the 30-day time span by both the MEMS gravimeter and gPhoneX are shown in Fig. 6. Excellent agreements are obtained with a correlation coefficient R of 0.957 between the two data sets. It can be seen that the semi-diurnal tidal cycle was clearly observed within a month, demonstrating a good long-term stability for the MEMS gravimeter. An additional Earth tides measurement within a time-span of 15 days, from Aug. 20, 2021 to Sep. 04, 2021, are shown in Note S2 of Supplemental Material, further validating the long-term stability of the MEMS gravimeter.

The results of other state-of-the-art MEMS gravimeters and accelerometers, as well as the proposed MEMS gravimeter are listed in Table 1. Within a stable pressure and temperature environment, our MEMS gravimeter exhibits an ultra-low noise floor and an excellent stability.

IV. Conclusion

In this work, the design considerations and system evaluations of a MEMS gravimeter are presented. The spring-mass structure showed an ultra-low self-noise floor, and a large linear range of >10000 mGal that is suitable for global deployment. By implementing a vacuum chamber, as well as an active temperature control system with a two-stage passive thermal insulation layer, the effects of the pressure and temperature have been greatly suppressed. Experimental results show that the pressure variation in the vacuum chamber tends to be linear of ~6 Pa/day after 30 days. The temperature control system shows a temperature noise of 0.4 mK/√Hz@1 mHz for the core area around the MEMS gravity sensor, giving a suppression of temperature fluctuations by 2 to 3 orders of magnitude within the 1×10^{-4} Hz to 1×10^{-2} Hz band. After the integration of the MEMS gravity sensor with the vacuum chamber and temperature control system, the Earth tides within a 30-day time span were successfully observed with a correlation coefficient of 0.957, providing an excellent long-term stability with a bias instability of ≤4 µGal within the 8 to 3000 s averaging time. The results represent one of the best performances so far in terms of stability for MEMS gravimeters, validating that a highly stable and sensitive MEMS gravimeter can be achieved by careful design considerations. Further miniaturizations and improvements of the MEMS gravimeter, including the implementation of a ceramic vacuum package and a bespoke FPGA board, can result in an increased portability and a reduction in cost, enabling MEMS gravimeters to be used for mineral exploration, geology and other geophysical applications.
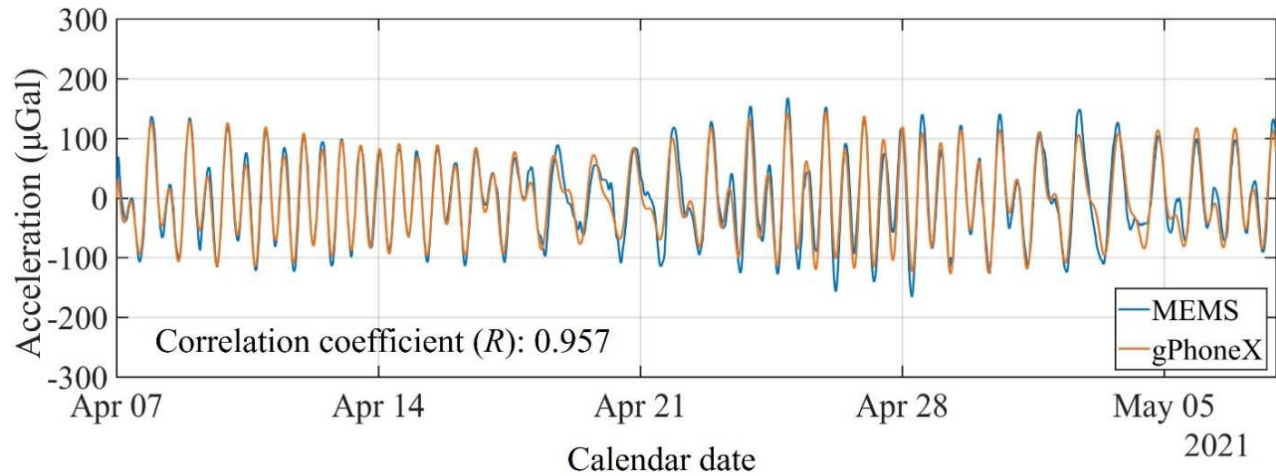
Fig. 6. Long-term Earth tides measurements with a time-span of 30 days from April 07, 2021 to May 07, 2021. The blue and orange series are signals measured by the MEMS gravimeter and a gPhoneX commercial gravimeter, respectively, with a correlation coefficient of 0.957.

TABLE I
COMPARISON OF THE PROPOSED MEMS GRAVIMETER WITH STATE-OF-THE-ART MEMS GRAVIMETERS AND ACCELEROMETERS

| Reference	Natural Frequency	Noise Floor	Temperature Environment	Bias Instability
[21]	7.35 Hz	18 μGal/√Hz@1 Hz	0.2 mK	8 μGal@~400 s <20 μGal@10-1000 s
[22]	~3.1 Hz	8 μGal/√Hz@1 Hz	N/A	13.5 μGal@20 s <20 μGal@10-1000 s
[24]	~1 kHz	100 μGal/√Hz@1 Hz	±250 μK@ 50°C	9 μGal@1000 s <50 μGal@10-1000 s
[25]	20 kHz	75 ng/√Hz@0.5 Hz	±0.01°C@ 45°C	17 ng@70 s <30 ng@10-1000 s
[40]	N/A	10 ng/√Hz@1 Hz	±0.001°C@ 40°C	7 ng@900 s <40 ng@10-1000 s
This work	~14 Hz	1.2 μGal/√Hz@1 Hz	0.4 mK/√Hz@1 mHz	3 μGal@80 s <8 μGal@10-1000 s

REFERENCES

[1] D. Sherlock, A. Toomey, M. Hoversten, *et al*., "Gravity monitoring of CO₂ storage in a depleted gas field: A sensitivity study," *Explor. Geophys.*, vol. 37, no 1, pp. 37-43, Mar. 2006.
[2] E. Gasperikova, D. Appriou, A. Bonneville, *et al*., "Sensitivity of geophysical techniques for monitoring secondary CO₂ storage plumes," *Int. J. Greenhouse Gas Control*, vol. 114, pp. 103585, Feb. 2022.
[3] M. N. Nabighian, M. E. Ander, V. J. S. Grauch, *et al*., "Historical development of the gravity method in exploration," *Geophys.*, vol. 70, no 6, pp. 63ND-89Nd, Nov. 2005.
[4] F. E. K. Ghomsi, R. Tenzer, E. Njinju, *et al*., "The crustal configuration of the West and Central African Rift System from gravity and seismic data analysis," *Geophys. J. Int.*, vol. 230, no 2, pp. 995-1012, Sep. 2022.
[5] D. Carbone, M. P. Poland, M. Diament, *et al*., "The added value of time-variable microgravimetry to the understanding of how volcanoes work," *Earth Sci. Rev.*, vol. 169, pp. 146-179, Jun. 2017.
[6] L. Xing, X. Niu, L. Bai, *et al*., "Monitoring groundwater storage changes in a karst aquifer using superconducting gravimeter OSG-066 at the Lijiang station in China," *Pure Appl. Geophys.*, pp,1-18, Apr. 2022.
[7] G. Berrino, "The state of the art of gravimetry in Italy," *Rendiconti Lincei. Scienze Fisiche e Naturali*, vol. 31, no 1, pp. 35-48, Oct. 2020.
[8] U. Riccardi, S. Rosat, J. Hinderer, "Comparison of the Micro-g LaCoste gPhone-054 spring gravimeter and the GWR-C026 superconducting gravimeter in Strasbourg (France) using a 300-day time series," *Metrologia*, vol. 48, no 1, pp. 28-39, Jan. 2011.
[9] D. D. Shin, C. H. Ahn, Y. Chen, *et al*., "Environmentally robust differential resonant accelerometer in a wafer-scale encapsulation process," in *2017 IEEE 30th International Conference on Micro Electro Mechanical Systems (MEMS)*, Las Vegas, NV, USA, Jan. 22-26, 2017, pp. 17-20.
[10] Q. Lu, J. Bai, K. Wang, *et al*., "Design, optimization, and realization of a high-performance MOEMS accelerometer from a double-device-layer SOI wafer," *J. Microelectromech. Syst.*, vol. 26, no 4, pp. 859-869, Aug. 2017.
[11] M. Zhao, K. Jiang, H. Bai, *et al*., "A MEMS based Fabry–Pérot accelerometer with high resolution," *Microsyst. Technol.*, vol. 26, no 6, pp. 1961-1969, Jun 2020.

[12] C. Li, B. Yang, X. Zheng, et al., "2 ng/√Hz-resolution optomechanical accelerometer employing a three-dimensional MEMS interferometer," Opt. Lett., vol. 47, no 7, pp. 1883-1886, Apr. 2022.

[13] T. Miao, X. Zhou, X. Wu, et al., "Nonlinearity-mediated digitization and amplification in electromechanical phonon-cavity systems," Nat. Commun., vol. 13, no 1, pp. 1-8, Apr. 2022.

[14] M. S. Weinberg, J. J. Bernstein, J. T. Borenstein, et al., "Micromachining inertial instruments," in Proc. SPIE 2879, 1996, Austin, TX, US. pp. 26-36.

[15] M. Elhoushi, J. Georgy, A. Noureldin, et al. "Motion mode recognition for indoor pedestrian navigation using portable devices," IEEE Trans. Instrum. Meas., vol. 65, no 1, pp. 208-221, Jan. 2016.

[16] S. Finkbeiner, "MEMS for automotive and consumer electronics," in 2013 Proceedings of the ESSCIRC (ESSCIRC), Bucharest, Romania, Sep. 16-20, 2013, pp. 9-14.

[17] W. Wu, J. Liu, J. Fan, et al., "A nano-g micromachined seismic sensor for levelling-free measurements," Sens. Actuators A Phys., vol. 280, no 1, pp. 238-244, Sep. 2018.

[18] B. A. Boom, "Acceleration sensing at the nano-g level: Development and characterisation of low-noise microseismometers for next generation gravitational wave detectors," Ph.D. dissertation, Department of Physics and Astronomy, Vrije Universiteit Amsterdam, Amsterdam, NL, 2020.

[19] W. T. Pike, I. M. Standley, S. B. Calcutt, et al., "A broad-band silicon microseismometer with 0.25 ng/rtHz performance," in 2018 IEEE Micro Electro Mechanical Systems (MEMS), Belfast, UK, Jan. 21-25, 2018, pp. 113-116.

[20] R. P. Middlemiss, A. Samarelli, D. J. Paul, et al., "Measurement of the Earth tides with a MEMS gravimeter," Nature, vol. 531, no 7596, pp. 614-617, Mar. 2016.

[21] A. Prasad, R. P. Middlemiss, A. Noack, et al., "A 19 day earth tide measurement with a MEMS gravimeter," Sci. Rep., vol. 12, no 1, pp. 13091, Jul. 2022.

[22] S. Tang, H. Liu, S. Yan, et al., "A high-sensitivity MEMS gravimeter with a large dynamic range," Microsyst. Nanoeng., vol. 5, no 1, pp. 1-11, Oct. 2019.

[23] X. Xu, Q. Wang, L. Yang, et al., "On the air buoyancy effect in MEMS-based gravity sensors for high resolution gravity measurements." IEEE Sens. J., vol. 21, no 20, pp. 22480-22488, Aug. 2021.

[24] A. Mustafazade, M. Pandit, C. Zhao, et al., "A vibrating beam MEMS accelerometer for gravity and seismic measurements," Sci. Rep., vol. 10, no 1, pp. 1-8, Jun. 2020.

[25] Z. Fang, Y. Yin, C. Chen, et al., "A sensitive micromachined resonant accelerometer for moving-base gravimetry," Sens. Actuators A Phys., vol. 325, pp. 112694, Jul. 2021.

[26] E. H. Klaassen, K. Petersen, J. M. Noworolski, et al., "Silicon fusion bonding and deep reactive ion etching: a new technology for microstructures," Sens. Actuators A Phys., A, vol. 52, no 1, pp. 132-139, Mar. 1996.

[27] W. T. Pike, A. K. Delahunty, A. Mukherjee, et al., "A self-levelling nano-g silicon seismometer," in SENSORS, 2014 IEEE, Valencia, Spain, Nov. 2-5, 2014. pp. 1599-1602.

[28] V. Josselin, P. Touboul, R. Kielbasa, "Capacitive detection scheme for space accelerometers applications," Sens. Actuators A Phys., vol. 78, no 2, pp. 92-98, Dec. 1999.

[29] C. H. Cho, "Characterization of Young's modulus of silicon versus temperature using a 'beam deflection' method with a four-point bending fixture," Curr. Appl Phys., vol. 9, no 2, pp. 538-545, Mar. 2009.

[30] M. A. Hopcroft, W. D. Nix, T. W. Kenny, "What is the Young's modulus of silicon?," J. Microelectromech. Syst., vol. 19, no 2, pp. 229-238, Apr. 2010.

[31] H. Watanabe, N. Yamada, M. Okaji, "Linear thermal expansion coefficient of silicon from 293 to 1000 K," Int. J. Thermophys., vol. 25, no 1, pp. 221-236, Jan. 2004.

[32] C. J. Bell, S. Reid, J. Faller, et al., "Experimental results for nulling the effective thermal expansion coefficient of fused silica fibres under a static stress," Classical Quantum Gravity, vol. 31, no 6, pp. 065010, Feb. 2014.

[33] IEEE Recommended Practice for Precision Centrifuge Testing of Linear Accelerometers, Standard IEEE Standard 836-2009, Institute of Electrical and Electronics Engineers, Sept. 2009.

[34] M. Zhang, S. Yan, Z. Deng, et al., "Cross-coupling coefficient estimation of a nano-g accelerometer by continuous rotation modulation on a tilted rate table," IEEE Trans. Instrum. Meas., vol. 70, pp. 1-12, Apr. 2021.

[35] L. G. Holcomb, "A direct method for calculating instrument noise levels in side-by-side seismometer evaluations," U.S. Geol. Surv. Open-File Report, 1989.

[36] S. Yan, Y. Xie, M. Zhang, Z. Deng, and L. Tu, "A subnano-g electrostatic force-rebalanced flexure accelerometer for gravity gradient instruments," Sensors, vol. 17, no. 11, pp. 2669, Nov. 2017.

[37] Q. Wang, Z. Li, H. Liu, et al., "MEMS microgravity measurement module with mano-g/Hz noise floor for spaceborne higher-level microgravity scientific experiment applications," ACS Appl. Electron. Mater., vol. 3, no 8, pp. 3379-3390, Aug. 2021.

[38] R. P. Middlemiss. "A practical MEMS gravimeter," Ph.D. dissertation, School of Physics & Astronomy, University of Glasgow, Glasgow, Scotland, 2016.

[39] N. El-Sheimy, H. Hou, X. Niu, "Analysis and modeling of inertial sensors using Allan variance," IEEE Trans. Instrum. Meas., vol. 57, no 1, pp. 140-149, Dec. 2007.

[40] G. Sobreviela-Falces, M. Pandit, A. Mustafazade, et al., "A MEMS vibrating beam accelerometer for high resolution seismometry and gravimetry", in 2021 IEEE Micro Electro Mechanical Systems (MEMS), Jan. 25-29, 2021, pp. 196-199.

Lujia Yang received the B.S. degree from Henan Polytechnic University in 2019. She is currently studying for the Ph.D. at Huazhong University of Science and Technology. Her research interest is in the field of MEMS accelerometers and gravimeters.
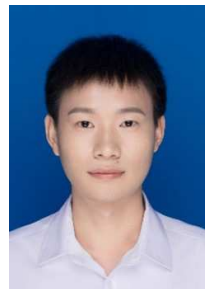
Xiaochao Xu received the B.S. degree in Physics from Hebei University of Technology, and the Ph.D. degree from Huazhong University of Science and Technology in 2022. His research interests include the MEMS inertial sensors, gravimeters, high stable temperature control and weak signal detection.

Qian Wang received the B.S degree from Henan University of Science and Technology in 2018 and the M.S degree from Huazhong University of Science and Technology in 2021. He is currently working at Avic Shanghai Aviation Electronic CO.LTD. His research interest is in the field of temperature control systems for high precision experimental physics.

Ji'ao Tian received the B.S. degree in 2017 and the M.S. degree in 2021, both from Huazhong University of Science and Technology. He is currently an R & D engineer of China State Shipbuilding Corporation Limited. His research interest is in the field of MEMS accelerometers.

Yanyan Fang received the B.S. degree from Henan University in 2018, and the M.S. degree from Huazhong University of Science and Technology in 2021. Since 2018, she has been engaged in the development of high-precision temperature control systems.

Chun Zhao Chun Zhao (S'14 - M'16 - SM'20) received B.Eng. degree from the Huazhong University of Science and Technology, Wuhan, China, in 2009; M.Sc. degree from Imperial College London, London, U.K., in 2011; and Ph.D. degree from the University of Southampton, Southampton, U.K., in 2016. From April 2015 to March 2016, he was a full time Research Scientist at Sharp Laboratories of Europe, Oxford, U.K. From April 2016 to August 2018, he was with the Department of Engineering, University of Cambridge, as a Research Associate in MEMS. Between September 2018 and December 2021, he was affiliated with the School of Physics, Huazhong University of Science and Technology, China, where he was an associate professor. Since February 2022, he has been a Lecturer in Microengineering at the Department of Electronic Engineering, University of York, UK. Dr. Zhao currently serves an Associate Editor of the IEEE Sensors Journal, and has served as the invited reviewer for several top journals in the field, including JMEMS, TIE, TUFFC and TCAS-I. His research interests include high resolution MEMS sensors, MEMS resonators, new materials for MEMS and new physics for MEMS (e.g. modal interactions and nonlinear effects).

Fangjing Hu received the B.Sc. and M.Sc. degrees from the University of Electronic Science and Technology of China (UESTC) in 2007 and 2010, respectively, and the Ph.D. degree from Imperial College London, U.K., in 2015, all in Electronic Engineering. He is currently an Associate Professor with the School of Physics, Huazhong University of Science and Technology, China. His research interests include MEMS sensors and applications. In 2016, he received the Eryl Cadwaladr Davies Prize for the best doctoral thesis in 2015, within the Department of Electrical and Electronic Engineering at Imperial College London. He has served as Reviewer for several top journals, including Advanced Functional Materials, Laser & Photonics Reviews, and Journal of Applied Physics.

Liangcheng Tu received the B.S. degree from Hubei University, in 1996, and the Ph.D. degree from the Huazhong University of Science and Technology (HUST), Wuhan, China, in 2006, all in physical science.
He is currently a full-time Professor with the School of Physics and Astronomy, Sun Yat-Sen University, and a part-time Professor with the School of Physics, HUST. His current research interests include lab gravitational experiments, gravity measurement technologies, and semiconductor device physics.